JMEPEG (2009) 18:1–7
DOI: 10.1007/s11665-008-9258-9

1059-9495/$19.00

Corrosion Properties and Morphology of Laser Melted Aluminum Alloy 8022 Surface

B.S. Yilbas, M. Khaled, and C. Karatas

(Submitted September 7, 2007; in revised form March 7, 2008)

Laser surface melting of aluminum alloy 8022 is considered and electrochemical studies of the laser-melted and as-received alloy surface are carried out. The surface morphology and metallurgical changes in the laser-melted region are examined using optical microscopy, electron scanning microscopy (SEM), and atomic force microscopy (AFM). Elemental changes in the specimens after the laser-melting process are examined using energy dispersive spectroscopy (EDS), and x-ray diffraction (XRD) is used for assessment of the compound formed after the laser-treatment process. Nitrogen is used as an assisting gas during the laser-melting process to prevent high-temperature oxidation reactions. It is found that the laser-melted surfaces is free from cracks and deep cavities. The oxygen diffusion in the surface region of the melt layer forms Al_2O_3 compound in the surface vicinity. The corrosion current increases significantly for the laser-melted specimens due to the irregular surface structure. AC impedance results showed a decrease in pores resistant and an increase in pores capacitance. In addition, the surface morphology resulting from the laser melting gives rise to pitting sites at the surface.

Keywords aluminum alloy, corrosion, laser, melting, pitting

1. Introduction

Aluminum alloys are widely used in industry due to their light weight and high thermal as well as electrical conductivities. However, the surface properties, such as hardness and wear resistance, of the alloy can be improved through control melting, coating, alloying, and chemical treatment techniques. Laser surface melting provides improved surface properties with localized affects. The requirement of the structural homogeneity and the large area of the treatment make laser processing difficult to realize (Ref 1). Moreover, the homogeneous structure in the surface region is essential for the corrosion protection. This is because of the non-uniform surface structure and the composition, due to non-uniform cooling rates, causes the large corrosion sites developed at the surface when the surface is exposed to the corrosive environment. Aluminum alloy 8022 is used in the corrosive environments due to its high corrosion resistance; however, the corrosion properties can be modified after the laser treatment process despite the fact that laser treatment improves the tribological properties of the surface. Consequently, investigation into the laser treatment of aluminum alloy 8022 and the assessment of the corrosion response of the laser-treated surface become essential.

B.S. Yilbas, Mechanical Engineering Department, KFUPM, Dhahran, Saudi Arabia; **M. Khaled**, Chemistry Department, KFUPM, Dhahran, Saudi Arabia; and **C. Karatas**, Engineering Faculty, Hacettepe University, Ankara, Turkey. Contact e-mail: bsyilbas@kfupm.edu.sa.

Considerable research studies were carried out to examine the laser treatment of aluminum alloy surfaces. The laser surface melting of aluminum alloy was investigated by Pokhmurska et al. (Ref 1). They indicated that the susceptibility to pitting corrosion of the laser-melted surface was not improved significantly as compared to that of as-received specimen. The intergranular corrosion and the intergranular stress corrosion cracking of the laser modified aluminum alloy surface were examined by Chigasaki et al. (Ref 2). They indicated that the intergranular corrosion and the intergranular stress corrosion cracking reduced significantly for the specimens treated by a laser beam. The laser-induced surface modification and electrochemical characteristics of the resulting surface of aluminum alloy were investigated by Kachurina et al. (Ref 3). They observed that the corrosion resistance of the alloy improved due to the oxide formation in the surface region. The laser treatment of aluminum alloy and the corrosion resistance of the surface were investigated by Watkins et al. (Ref 4). They showed from the electrochemical tests that the micro-segregation within the overlapping areas of the laser irradiated spots lead to the initiation of the pitting corrosion at the alloy surface. The effect of laser surface melting on the corrosion and cavitations behavior of aluminum alloy was investigated by Tang et al. (Ref 5). They indicated that the shift in the corrosion potential under the cavitations revealed the difference in the relative dominance effect of the cavitations on the cathodic and anodic reactions on the laser-treated specimens. The effect of excimer laser melting on the intergranular corrosion cracking of aluminum alloy was studied by Yue et al. (Ref 6). They indicated that the polarization resistance of the laser-treated specimens was at least two orders of magnitude higher than that of the untreated specimens. The corrosion protection of aerospace aluminum alloys with laser surface melting was investigated by Davenport et al. (Ref 7). They showed that the laser-treated layer demonstrated the cathodic current density for the laser-melted surface was typically half of

that of the untreated surface. The corrosion resistance of the aluminum composite treated by a laser beam was investigated by Hu et al. (Ref 8). They showed that the laser power intensity influenced the corrosion resistance of the surface; in this case, the specimen with 700 W laser treatments exhibited a greater resistance to the corrosion than the other specimens. The excimer laser interaction with aluminum alloy was studied by Koutsomichalis and Kefalidou (Ref 9). They demonstrated that the laser-treated aluminum alloy exhibited a higher corrosion resistance. Laser surface treatment of aluminum alloy and corrosion fatigue resistance were examined by Xu et al. (Ref 10). They showed that the total fatigue life of the alloy increased noticeably after the laser surface treatment, which was due to the excellent resistance to the pitting corrosion of the laser-treated specimens. The large area of laser surface treatment of aluminum alloys for pitting corrosion protection was carried out by Chong et al. (Ref 11). They indicated that the pitting potential of the surface was enhanced for the laser-treated alloys.

In the present study, laser melting of aluminum alloy 8022 is carried out and the corrosion responses of the laser-treated and as-received surfaces are examined. The surface morphology and the metallurgical changes in the laser-treated region are examined using optical microscopy, electron scanning microscopy (SEM), and atomic force microscopy (AFM). The elemental composition and the compounds formed in the laser melted layer are investigated using energy dispersive spectroscopy (EDS), and the x-ray diffraction (XRD) technique is employed for the assessment of the compounds formed after the laser-treatment process.

2. Experimental

The CO_2 laser (LC-ALPHAIII) delivering nominal output power of 2 kW at pulse mode with different frequencies was used to irradiate the workpiece surface. The nominal focal length of the focusing lens was 127 mm. Nitrogen assisting gas emerging from the conical nozzle and co-axially with the laser beam was used. The workpiece surface was scanned at a constant speed by a laser beam. Laser treatment conditions are given in Table 1.

An aluminum alloy 8022 was used as the workpiece material. The elemental composition of the alloy is given in Table 2.

A corrosion flat cell from Princeton Applied Research (K0235) was used for all electrochemical experiments described. The reference electrode was an Ag/AgCl electrode from Bioanalytical systems. The aluminum substrate and the laser-treated specimens were the working electrodes under investigations. The aluminum substrate was a plate of dimensions $2 \times 5 \times 0.2$ cm where 1 cm^2 area was exposed to the 0.7 M NaCl solution in the electrochemical cell. The molarity was selected to be 0.7 M to simulate the behavior of the extreme saline environments. Electrochemical polarization experiments were performed using the PCI4/300 Gamry potentiostat. The DC corrosion techniques software, DC105, supplied also by Gamry, was used to control the potentiostat and analyze the Tafel region. The electrochemical impedance experiments were performed using the previous Gamry potentiostat. The EIS impedance technique software, EIS300, supplied by Gamry also used to control the potentiostat and analyze the bode plot. The impedance experiments are carried out using plates of the same dimensions as in the case of electrochemical polarization experiments, where 1 cm^2 area was exposed to the 0.7 M NaCl solution in the electrochemical cell. The initial and final frequencies were 300,000 and 0.01 Hz, respectively. The untreated aluminum specimen were degreased in isopropanol and polished with emery paper with grits 200-1200, then rinsed thoroughly with deionized water. The laser-treated aluminum substrate was washed with isopropanol and followed by deionized water.

The data sampling started after ensuring a potential drift of less than 0.1 mV/s. The experiments were repeated in triplicate to ensure reproducibility of the voltammograms. The scan rate was 0.1667 mV/s.

Material characterization of the laser-treated surfaces is carried out using SEM, EDS, and XRD. Jeol 6460 electron microscopy is used for SEM and EDS examinations and Broker D8 Advanced having MoKα radiation is used for XRD analysis. A typical setting of XRD was 40 kV and 30 mA. The morphology of the laser-melted surfaces was performed using a 5100 AFM/SPM Microscope by Agilent in contact mode. The tip was made of silicon nitride probes (r = 20-60 nm) with a manufacturer specified force constant, k, of 0.12 N/m.

3. Results and Discussion

Laser melting of aluminum alloy 8022 is carried out and the corrosion responses of the laser-melted and as-received surfaces are investigated. The surface morphology and the metallurgical changes in the melt region are examined.

Figure 1 shows SEM micrographs of the top and the cross-sectional views of the laser-melted regions. The appearance of

Table 1 Laser-assisted surface treatment conditions

Scanning speed, mm/min	Power, W	Peak power, W	Frequency, Hz	Nozzle gap, mm	Nozzle diameter, mm	Gaussian parameter, mm	Focus setting, mm	N_2 pressure, kPa
2000	320	2000	1000	0.5	1.5	0.55	127	300

Table 2 Elemental composition of aluminum alloy 8022 (wt.%) obtained from EDS

Al	Cr	Fe	Mn	O	Si	Ti	V	Zn
Balance	Max. 0.1	6.2-6.8	Max. 0.1	0.05-0.2	1.2-1.4	Max. 0.1	0.4-0.8	Max. 0.25

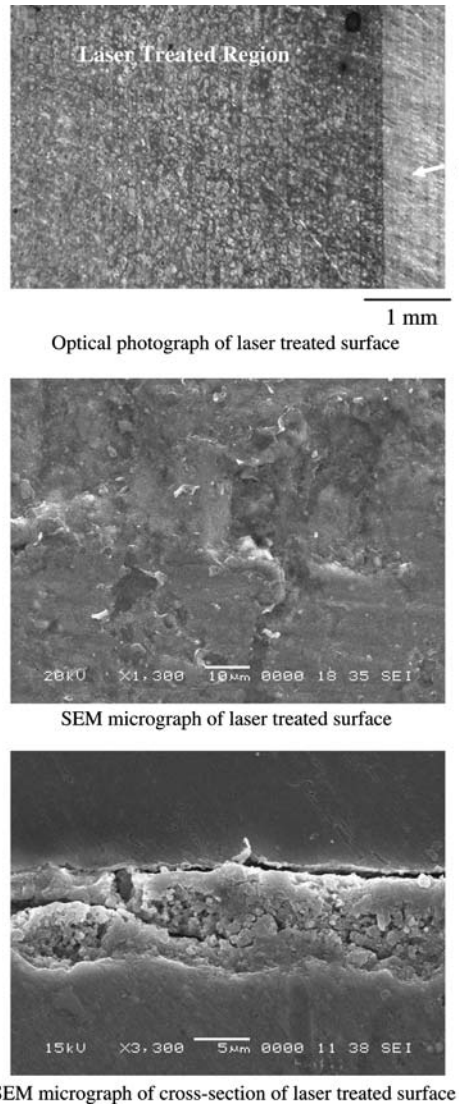

Fig. 1 Optical photograph and SEM micrographs of laser-treated surface

brownish color of the melted surface indicates the presence of the AlN compound in the surface region. This is because of the use of nitrogen assisting gas during the laser-melting process. Consequently, the formation of AlN is due to the reaction of liquid aluminum with nitrogen (N^{-3}), similar to the observation reported in the previous study (Ref 12). It is evident from the top view of the laser-melted surface that the surface roughness increases significantly. This can also be observed from Fig. 2, in which the surface roughness of the laser-melted and as-received specimen surfaces are shown. However, close examination of the SEM micrograph reveals that no-crack site is evident and locally scattered shallow cavities and irregular morphology occur at the surface. This is because of some small evaporation of the surface that takes place during the melting process. Moreover, no loose or partially detached particle at the surface is observed. In the case of the specimen cross-sectional view, a compact Al_2O_3 layer is formed at the surface and particulates like structure is formed in the layer below the surface. In addition, no distinct heat-affected layer is observed below the melt layer. The laser melt layer extends to 12 µm

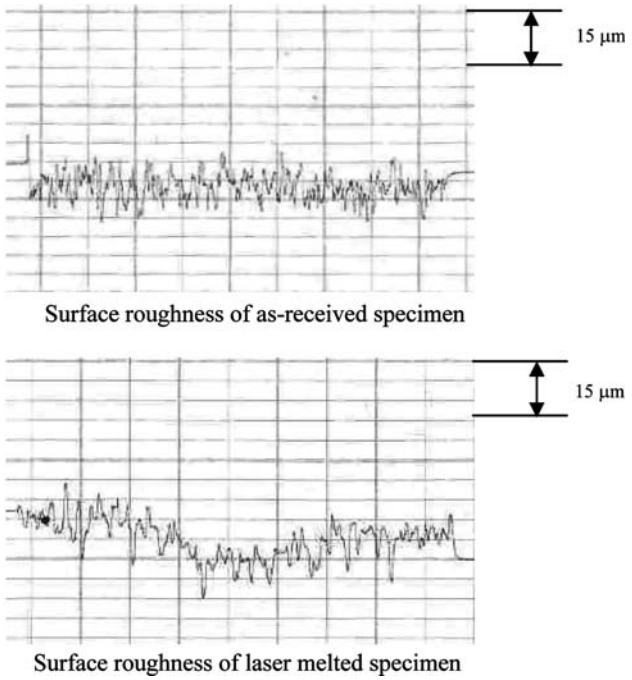

Fig. 2 Surface roughness of as-received and laser-melted specimens

Table 3 EDS results for two depths below the surface of the laser-melted specimen

Depth	Al	O	Si	Fe
3 µm	Balance	24.30	1.19	6.44
7 µm	Balance	12.97	1.14	6.46

below the surface and the melt layer appears to be uniform, provided that the irregular topology results in the large surface roughness. The EDS analysis reveals that oxygen concentration reduces in this region (Table 3). This is because of the oxygen saturation in the surface vicinity, which acts as a surface barrier for oxygen diffusion. Although oxygen diffusion coefficient for aluminum is small (Ref 13), the duration of the CO_2 laser heating is longer than that of the pulsed lasers. Consequently, oxygen diffusion in the melt layer as well as the surface tension driven flow in the melt pool (Ref 14) enhances the oxygen concentration in the melt layer. Figure 3 shows the XRD results of the laser-melted specimen. The formations of Al_2O_3 and SiO_2 are evident after the laser-treatment process. In addition, AlN compound is also evident from the XRD results, i.e., use of N_2 assisting gas during the laser-melting process is responsible for AlN formation in the melt layer.

Figure 4 shows the bode plots of the untreated and laser-treated aluminum specimen consequently in 0.7 M NaCl. The paint model is used for analyzing the obtained bode plots and data are shown in Table 4. It should be noted the data presented in Table 4 are obtained from the EIS impedance software, EIS300, supplied by Gamry. It is noted that the obtained bode plots consists of two times constant and two different slopes which belong to coating capacitance and double layer capacitance, respectively. It is observed that pore resistance (R_{po}) for untreated sample 3.799×10^3 Ω is greater than that for treated one 1.799×10^3 Ω. This indicates that the treatment affected the

assumed coat on the surface and increased the porosity, which in turn decreased the porosity resistance. It is also noted that the coating capacitance (C_c) increased from 14.51×10^{-6} F for the untreated aluminum to 28.01×10^{-6} F for the laser-treated specimen, which indicates an increase in the exposed surface area. Furthermore, the decrease of the charge transfer resistance from 174.3×10^{-3} Ω to 68.31×10^{-3} Ω and increase of the double layer capacitance from 198.8×10^{-6} F to 353.5×10^{-6} F of treated sample indicates that surface changes are occurring on the sample surface as a result of leaser treatment.

Potentiodynamic curves and corrosion parameters are shown in Fig. 5 and Table 5, respectively. It is noted from Fig. 5 that the corrosion potential of the laser-treated aluminum specimen decreased to −139 mV compared to 29 mV for the untreated specimen. The corrosion current and corrosion rates measurements showed an increase by a factor close to ten. This correlates with the pervious results of impedance which showed an increase in pores surface and hence increase exposure to the corrosive solution. Furthermore, the treated aluminum specimen does not show passivation at lower potentials, whereas the untreated specimen show a semi-passive region at low potentials at lower currents compared to the laser-treated specimen.

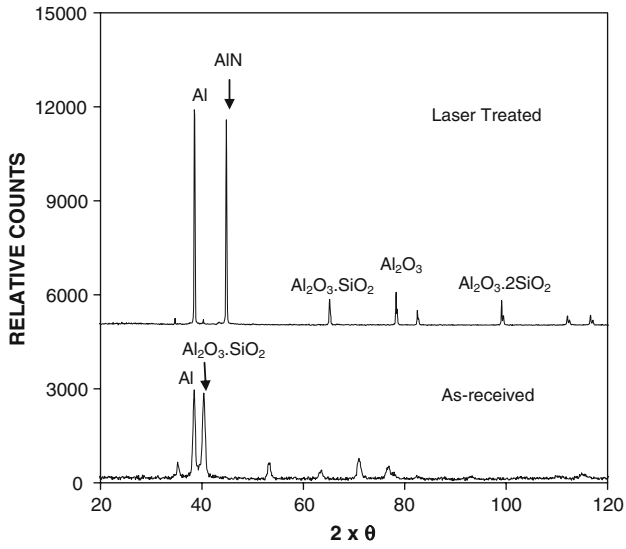

Fig. 3 XRD results for laser-melted and as-received specimens

Figure 6 shows the SEM micrographs of as-received and laser-melted as well as electrochemically tested surfaces. The micrographs show that the as-received and the laser-melted surface suffered from the severe corrosion attacks despite the fact that the laser-melted surface has rich oxygen content, which is expected to be resistant to the corrosion. However, due to the increased surface area as a result of the laser-melting process, the area subjected to the electrolytic solution becomes large. In addition, the irregular surface morphology enhances the crevice corrosion at the surface. In this case, the irregular surface structure acts as the sites for the crevice corrosion. The irregular structure developed after the laser treatment can also be seen in Fig. 7, in which the AFM micrographs are shown. Although the height of the irregular structure is small, it acts like a semi closed-loop site for the corrosion attack. Moreover, the specimen surface suffers from the initial corrosion attack during the electrochemical tests; in which case, the gas bubbles appear instantaneously. This shows the heterogeneity of electrochemical activities at the surface, i.e. some constituent particles act as cathodes to enhance the formation of hydrogen bubbles (Ref 6). Consequently, prolonging the corrosion time results in growing pit sizes and merging with the neighboring pits producing large surface defects. When damage size grows

Table 4 The bode plots data

Parameter	$R_{po}\times10^{-3}$ Ω	$C_c\times10^{6}$ F	$R_f\times10^{3}$ Ω	$C_f\times10^{6}$ F
Untreated	3.799	14.51	174.3	198.8
Treated	1.799	28.01 F	68.31	353.5

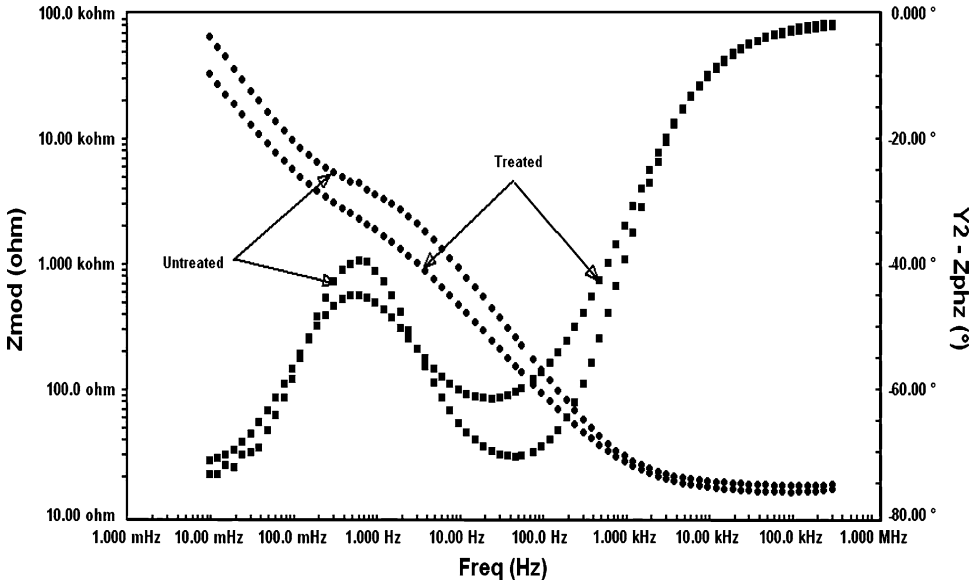

Fig. 4 The bode plots for the laser-melted and as-received aluminum samples in 0.7 M NaCl

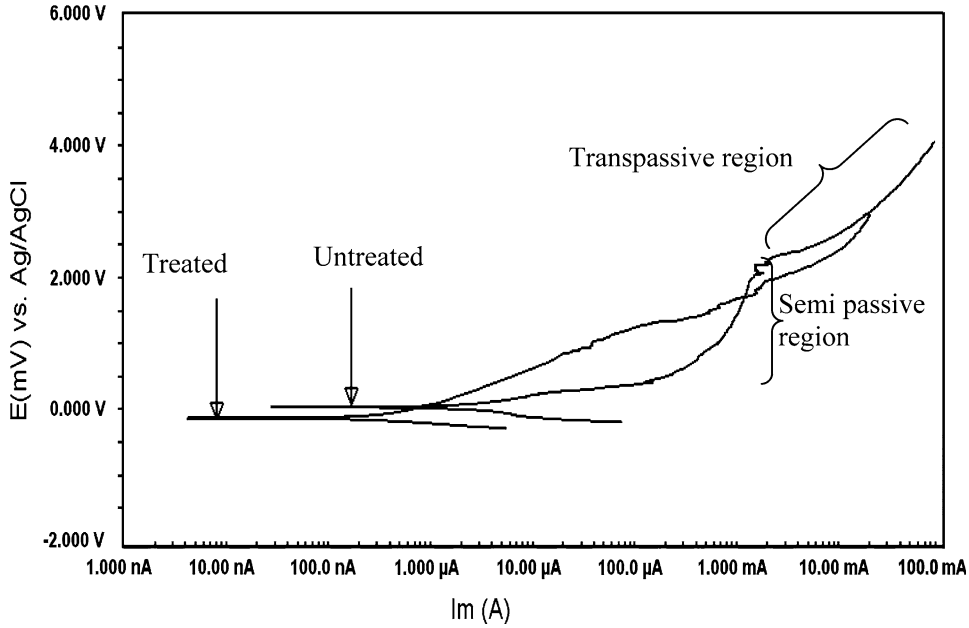

Fig. 5 Potentiodynamic plot for the laser-melted and as-received aluminum alloy specimens vs. Ag/AgCl in 0.7 M NaCl at a scan rate of 0.1667 mV/s

Table 5 Corrosion parameters extracted from Tafel region for untreated and laser-treated Al in 0.7 M NaCl

File	β_a, V/decade	β_c, V/decade	I_{corr}, µA/cm^2	E_{corr}, mV	CR, µmpy
Untreated	0.368	0.126	0.273	26	0.121
Treated	0.294	0.251	2.92	−139	1.3

to the critical size, the stress concentration and hydrogen embrittlement become important. This, in turn, initiates the micro-cracks reaching the grain boundaries; as a consequence, the grain boundaries become active corrosion paths. In this case, totally damaged grain boundaries and segregated grain is observed at the pit sites (Fig. 8).

4. Conclusion

Laser melting of aluminum alloy 8022 surface is considered and AC impedance spectroscopy and potentiodynamic experiments of the laser-melted as well as the as-received surfaces are investigated. The surface morphology and metallurgical changes in the laser-melted layer are examined using optical microscopy, SEM, EDS, XRD, and AFM. It is found that laser melting produces relatively rougher surface than the as-received sample surface, which yielded a decrease in pore resistance and increase in pore capacitance. Locally scattered shallow cavities are observed at the laser-melted surfaces. This occurs because of some small partial evaporation of the surface during the laser-melting process. However, no-crack and defect sites, such as large cavities and voids, are observed at the laser-melted surfaces. Oxygen diffusion in the surface region is high and the oxide compounds are formed in the surface region as well as below the surface. The possible explanation for the formation of the oxide compounds below the surface is the

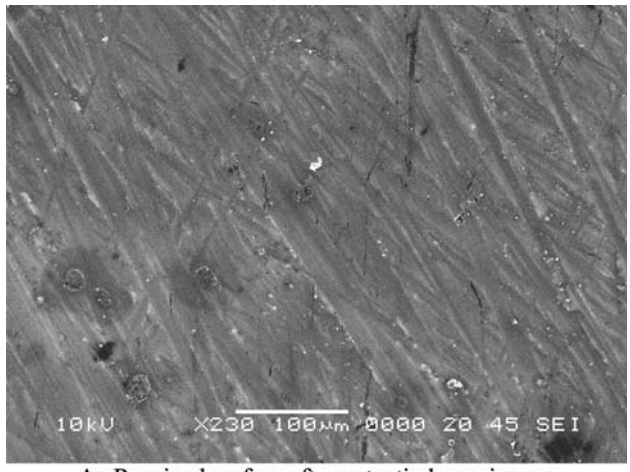

Fig. 6 SEM micrographs of as-received and laser-treated surfaces after the electrochemical tests

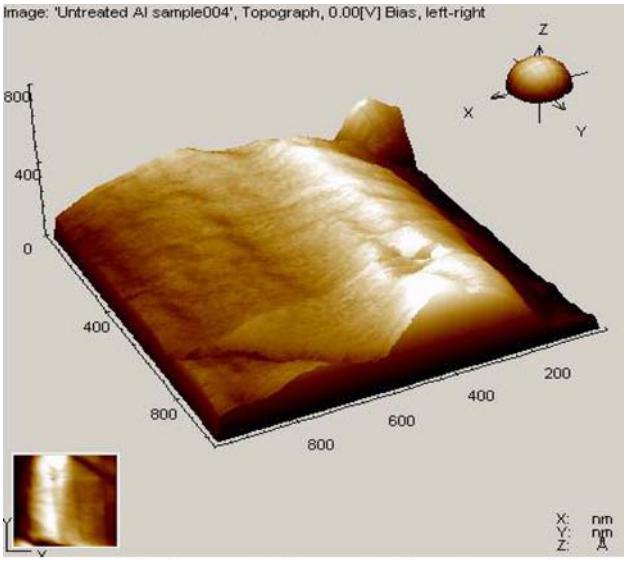

AFM micrograph of as-received specimen surface

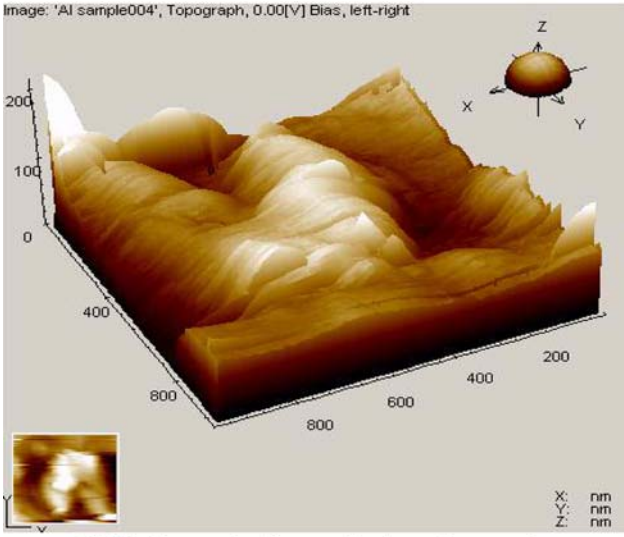

AFM micrograph of as-received specimen surface

Fig. 7 AFM micrographs of as-received and laser-melted surfaces

surface tension driven flow, which carries oxygen from the surface region to the melt pool during the long heating duration. The laser-melted region is in a compact structure at the surface; however, particulate type structure is formed below the surface. The compound formed in this region is mainly Al_2O_3 and AlO. The laser melting of the surface results in increased capacitance of the specimens indicating the increased surface area. The charge transfer resistance of the specimen as well as the corrosion current increase after the laser melting process. In addition, the laser-melted specimens do not show passivation at lower potentials, whereas the as-received specimens show a semi-passive region at low potential. The irregular surface morphology resulting from the laser melting process gives rise to the severe pitting sites at the surface. The hydrogen bubbles appear instantaneously in the initial corrosion sites at the surface, which, in turn, indicates the heterogeneity of the electrochemical activities at the surface. Due to the corrosion paths at the grain boundaries, segregated grain at the pit sites is observed.

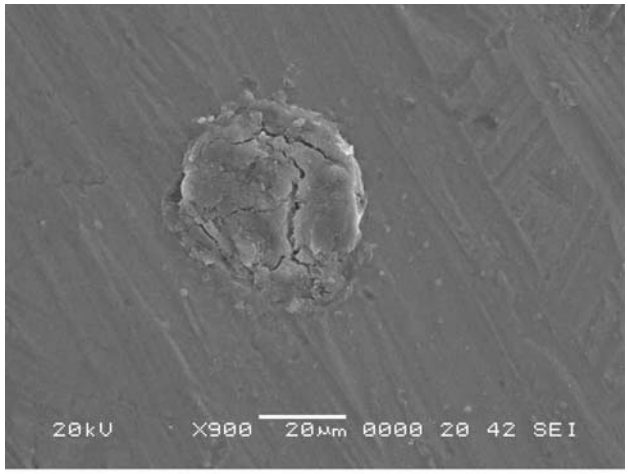

Formation of initial pit site

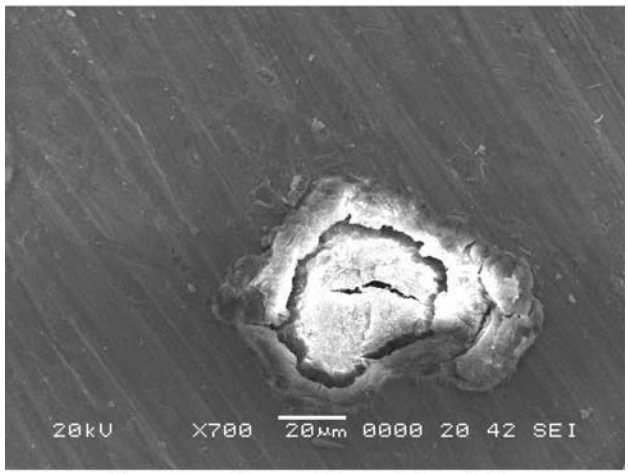

Corrosion path around the grain boundaries

Fig. 8 SEM micrographs of pit site initiation and segregated grain due to corrosion activities around the grain boundaries

Acknowledgments

The authors acknowledge the support of King Fahd University of Petroleum and Minerals, Dhahran, Saudi Arabia, Hacettepe University in Turkey, and Karmetal AS.

References

1. H. Pokhmurska, L. Kwiatkowski, W. Kalita, and J. Hoffman, Corrosion Behavior of Laser-Remelted Aluminium Alloy, *Proc. SPIE*, 2003, **5229**(1), p 260–265
2. M. Chigasaki, S. Matsushita, J. Kuniya, and T. Kato, Corrosion Resistance of Laser-Modified Surface of Alloy 600, Zairyo to Kankyo, *Corros. Eng.*, 1999, **48**(4), p 207–213
3. O. Kachurina, T.L. Metroke, and K. Dou, Laser-Induced Electrochemical Characteristics of Aluminum Alloy 2024-T3, *J. Laser Appl.*, 2004, **16**(1), p 46–51
4. K.G. Watkins, Z. Liu, M. McMahon, R. Vilar, and M.G.S. Ferreira, Influence of the Overlapped Area on the Corrosion Behaviour of Laser Treated Aluminum Alloys, *Mater. Sci. Eng. A: Struct. Mater.*, 1998, **252**(2), p 292–300
5. C.H. Tang, F.T. Cheng, and H.C. Man, Laser Surface Alloying of a Marine Propeller Bronze Using Aluminum Powder: Part II Corrosion and Erosion-Corrosion Synergism, *Surf. Coat. Technol.*, 2006, **200**, p 2594–2601

6. T.M. Yue, C.F. Dong, L.J. Yang, and H.C. Man, The Effect of Laser Treatment on Stress Corrosion Cracking Behavior of 7075 Aluminum Alloy, *Mater. Lett.*, 2004, **58**, p 630–635
7. A.J. Davenport, N.P.C. Tareelap, B.J. Connolly, S.W. Williams, E. Siggs, and D. A. Price, Corrosion Protection of Aerospace Aluminum Alloys with Laser Surface Melting. Meeting Abstracts, v MA 2005-02, 208th Meeting of The Electrochemical Society – Meeting Abstracts, 2005, p 551
8. J. Hu, G. Liu, Z.J. Li, and L.C. Kong, Improvement in the Corrosion Resistance of Al18B4O33w/2024Al Composite by Laser Surface Treatment, *Appl. Surf. Sci.*, 2007, **253**(10), p 4524–4530
9. A. Koutsomichalis and A. Kefalidou, Excimer Laser Interactions with an Aluminum Alloy, *J. Laser Appl.*, 1996, **8**(5), p 247–250
10. W.L. Xu, T.M. Yue, H.C. Man, and C.P. Chan, Laser Surface Melting of Aluminium Alloy 6013 for Improving Pitting Corrosion Fatigue Resistance, *Surf. Coat. Technol.*, 2006, **200**(6–17), p 5077–5086
11. P.H. Chong, Z.L. Liu, P. Skeldon, and G.E. Thompson, Large Area Laser Surface Treatment of Aluminum Alloys for Pitting Corrosion Protection, *Appl. Surf. Sci.*, 2003, **208–209**, p 399–404
12. A. Joshi, C.R. Shastry, and M. Levy, Effect of Heat Treatment on Solute Concentration at Grain Boundaries in 7075 Aluminum Alloy, *Metall. Trans. A*, 1981, **12A**(6), p 1081–1088
13. M. Guillodoa, J.M. Bassatb, J. Fouletiera, L. Dessemonda, and P. Del Gallo, Oxygen Diffusion Coefficient and Oxygen Exchange Coefficient of BIMEVOX.10 (ME=Cu, Co) Ceramic Membranes, *Solid State Ionics*, 2003, **164**, p 87–96
14. J. Srinivasan and B. Basu, A Numerical Study of Thermocapillary Flow in a Rectangular Cavity During Laser Melting, *Int. J. Heat Mass Transf.*, 1986, **29**(4), p 563–572